Galactic foreground contribution to the BEAST CMB Anisotropy Maps

Jorge Mejía [1] Marco Bersanelli [2] Carlo Burigana [3] Jeff Childers [4] Newton Figueiredo [5] Miikka Kangas [4] Philip Lubin [4] Davide Maino [2] Nazzareno Mandolesi [3] Josh Marvil [3] Peter Meinhold [4,6] Ian O'Dwyer [7] Hugh O'Neill [3] Paola Platania [2] Michael Seiffert [8] Nathan Stebor [3] Camilo Tello [1] Thyrso Villela [1] Benjamin Wandelt [7] Carlos Alexandre Wuensche [1]

mejia@das.inpe.br

ABSTRACT

We report limits on the Galactic foreground emission contribution to the Background Emission Anisotropy Scanning Telescope (BEAST) Ka- and Q-band CMB anisotropy maps. We estimate the contribution from the cross-correlations between these maps and the foreground emission templates of an Hα map, a de-striped version of the Haslam et al. 408 MHz map, and a combined 100 μm IRAS/DIRBE map. Our analysis samples the BEAST $\sim 10^\circ$ declination band into 24 one-hour (RA) wide sectors with $\sim$ 7900 pixels each, where we calculate: (a) the linear correlation coefficient between the anisotropy maps and the templates; (b) the coupling constants between the specific intensity units of the templates and the antenna temperature at the BEAST frequencies and (c) the individual foreground contributions to the BEAST anisotropy maps. The peak sector contributions of the contaminants in the Ka-band are of 56.5% free-free with a coupling constant of 8.3 ± 0.4 μK/R, and 67.4% dust with 45.0 ± 2.0

[1]Instituto Nacional de Pesquisas Espaciais, Divisão de Astrofísica, Caixa Postal 515, 12210-070 - São José dos Campos, SP, Brazil

[2]Dipartimento di Fisica, Universit degli study di Milano, via Celoria 16, 20133 Milano, Italy

[3]IASF-CNR sezione di Bologna, via P.Gobetti, 101, 40129 Bologna, Italy

[4]Physics Department, University of California, Santa Barbara, CA 93106

[5]Universidade Federal de Itajubá, Departamento de Física e Química, Caixa Postal 50, 37500-903 - Itajubá, MG, Brazil

[6]University of California, White Mountain Research Station, CA 93514

[7]Astronomy Department, University of Illinois at Urbana-Champaign, IL 61801-3074

[8]Jet Propulsion Laboratory, California Institute of Technology, Oak Grove Drive, Pasadena, CA 91109

μK/(MJy/sr). In the Q-band the corresponding values are of 64.4% free-free with 4.1 ± 0.2 μK/R and 67.5% dust with 24.0 ± 1.0 μK/(MJy/sr). Using a lower limit of 10% in the relative uncertainty of the coupling constants, we can constrain the sector contributions of each contaminant in both maps to $< 20\%$ in 21 (free-free), 19 (dust) and 22 (synchrotron) sectors. At this level, all these sectors are found outside of the $|b| = 14.6^\circ$ region. By performing the same correlation analysis as a function of Galactic scale height, we conclude that the region within $b = \pm 17.5^\circ$ should be removed from the BEAST maps for CMB studies in order to keep individual Galactic contributions below $\sim 1\%$ of the map's rms.

Subject headings: cosmology: observation, cosmic microwave background; interstellar medium

1. INTRODUCTION

The study of the anisotropies in the Cosmic Microwave Background Radiation (CMB) angular distribution represents one of the most important and active areas in Cosmology today. Measurements of the CMB anisotropies provide an important probe to understand the mechanisms of structure formation in the early Universe. Unfortunately, these measurements are hampered by Galactic and extragalactic emissions which limit the accuracy of the measured CMB power spectrum. As for Galactic contribution, diffuse emission is mainly due to synchrotron, free-free (thermal Bremsstrahlung) and dust emissions. Thus, it is important to quantify the precise level of these contaminating foregrounds in order to distinguish them from the cosmological signal. The clear identification of the contribution of each individual contaminant of the CMB signal is a challenging astrophysical task.

Below ~ 50 GHz, the primary Galactic foreground contaminants are synchrotron and thermal Bremsstrahlung emission. Their spectral signature, $T(\nu) \approx \nu^{-\beta}$, differ significantly from that of CMB fluctuations, since $\beta_{synch} \simeq 2.7$ and $\beta_{ff} \simeq 2.1$. Therefore, multi-frequency measurements with a large enough signal-to-noise ratio can distinguish between foreground and CMB fluctuations. Above ~ 50 GHz, the primary contaminant is interstellar dust emission, whose spectral shape is well fitted by an expression of the type $I_\nu \propto \nu^\beta B_\nu(T_d)$. At these frequencies, dust emission can also be distinguished from CMB fluctuations by its distinct spectral signature ($\beta_{dust} \simeq 1.5 - 2.0$) in multi-frequency observations. Recently, an additional component, correlated with dust emission, has been proposed (Draine & Lazarian 1998) but its existence and nature is still matter of discussion. Since spatial variability of β_{synch} and β_{dust} is quite significant, cross-correlation techniques between CMB maps and Galactic foreground templates have been employed recently in order to estimate the con-

tribution of Galactic foregrounds to CMB anisotropy data sets (e.g. Banday et al. 2003; Bennett et al. 2003; Hamilton & Ganga 2001; de Oliveira-Costa et al. 1999).

In this paper we evaluate the Galactic emission contribution to the BEAST (Background Emission Anisotropy Scanning Telescope) CMB anisotropy maps at 30 GHz and 41.5 GHz (Meinhold et al. 2003). We use a cross-correlation approach between the $\simeq 10^\circ$ wide declination band observed by BEAST in the Northern Hemisphere and the corresponding sky coverage in: (a) the Finkbeiner et al. (2003) all-sky map of Hα as a template for the free-free emission; (b) the Platania et al. (2003) de-striped version of the 408 MHz map (Haslam et al. 1982) as a template for the Galactic synchrotron emission and (c) a 100 μm combined IRAS/DIRBE dust template (Schlegel, Finkbeiner & Davis, 1998) for the dust emission. In the case of the free-free contribution, we compare our results with those obtained by Dickinson et al. (2003). In Section 2 we briefly describe the BEAST experiment. Section 3 presents the BEAST maps and discusses the foreground templates. We describe the method for evaluating the Galactic contamination in the BEAST maps in Section 4, while Section 5 discusses the analysis and results of this work.

2. THE BEAST TELESCOPE

The BEAST instrument (Childers et al. 2004; Figueiredo et al. 2004) is a 1.9-meter effective aperture off-axis Gregorian telescope configured with a 6-element Q-band (38-45 GHz; 23 ± 1 arcmin FWHM) and 2-element Ka-band (26-36 GHz; 28 ± 2 arcmin FWHM) focal plane array, and a modulating tilted flat mirror between the primary mirror and the sky. The instrument is currently acquiring data in Barcroft, CA, USA, at the White Mountain Research Station (WMRS) of the University of California at an altitude of ~ 3800 m. The spatial modulation provided by the movement of the tilted flat mirror results in an ellipsoidal scan of the sky with an $\sim 10^\circ$ major axis. Combined with the daily modulation due to the rotation of the Earth, BEAST scans a full 24-hour long declination band between +33 deg and +42 deg.

BEAST was designed to map the CMB with large sky coverage and high angular resolution. It was specifically conceived to make well connected maps through its scanning strategy. The range of frequencies covered by BEAST can help discriminate between the CMB signal and the Galactic foregrounds. The BEAST maps complement the Wilkinson Microwave Anisotropy Probe (WMAP) mission in several ways. For instance, BEAST measurements in the Q-band are of higher resolution than in WMAP, so we should be more sensitive to point sources. By measuring the CMB with high sensitivity and resolution over a limited region of the sky, we can get a better understanding of foregrounds to help disentangle the

individual Galactic contaminants. BEAST can also be adapted to allow fundamental studies of the S-Z effect on a large number of clusters, study dusty galaxies and their foreground contaminating role, and extend its multipole coverage.

3. BEAST AND FOREGROUND MAPS

The data used in this work correspond to ∼680 hours of observations taken between July 2001 and October 2002. An in-depth discussion of the observational strategy, the data processing procedure, and the map-generating pipeline is presented in Meinhold et al. (2003). During the acquisition process, the amplified output of each radiometer was AC-coupled with a high-pass time constant of 15 seconds. The raw data were binned into 250 sky positions per revolution of the modulating flat mirror and the first-order atmospheric contribution was eliminated by folding and subtracting the low frequency envelope in one-hour long data sets. A 10-Hz high-pass filter was applied to the resulting time-ordered data (TOD) in order to remove any remaining low frequency contribution of the $1/f$ noise, which is dominant in this region of the spectrum. The pointing coordinates were translated into HEALPix (Górski et al. 1999) pixel indexes to constitute the final BEAST maps per hour and per channel. These individual maps were co-added to obtain the final BEAST maps at 30 GHz and 41.5 GHz. Each BEAST map consists of $\sim 2 \times 10^5$ pixels (in HEALPix $N_{side} = 512$ pixelization) covering the entire declination band between $33^\circ < \delta < 42^\circ$. In this work, the region limited by $|b| = 10^\circ$ was removed considering that its complexity avoids any reasonable analysis. The resulting Ka-band map is shown in Figure 1 and the Q-band map in Figure 2.

The Galactic emission model we used for tracing the free-free component is the recently released compilation of Finkbeiner (2003) of an all-sky map of Hα with observations from WHAM (Reynolds et al. 2002), VTSS (Dennison et al. 1998) and SHASSA (Gaustad et al. 2001). As a tracer of Galactic synchrotron emission we used the 408 MHz map of Haslam et al. (1982). Finally, to model the thermal dust emission of the Galaxy we used a 100 μm combined IRAS/DIRBE map (Schlegel, Finkbeiner & Davis 1998; Finkbeiner, Davis & Schlegel 1999).

The three foreground maps were binned to the $N_{side} = 512$ HEALPix pixelization resolution and, then, processed by a BEAST experiment simulator, which samples, individually, each foreground map following the sequence of pixels observed by the BEAST telescope during a typical working day, in 1-hour time sets in the same manner the raw data are recorded. This procedure effectively reproduces the BEAST scanning pattern of the sky onto the foreground maps as if each Galactic component were to be the only source in the sky. The resulting TODs were then processed following exactly the same map-making pipeline as

with the BEAST raw data, described in the previous paragraph, to produce BEAST-like templates of the Galactic emission tracers.

The pipeline to produce BEAST-like foreground templates can be summarized as follows:

- selection of the appropriate templates,
- convolution of the original templates with the proper smooth function,
- appropriate binning and processing of the individual templates according to BEAST pointing,
- subtraction of the low frequency envelope and 10-Hz highpass filtering of the 1-hour long "template TOD",
- processing of the "template TOD" into a foreground template map in the same way as described in Meinhold et al. (2003).

4. METHOD

In order to analyze the foreground contribution to the BEAST CMB anisotropy maps, we considered a BEAST map, T_{BEAST}, to be a linear superposition of the actual CMB anisotropy distribution, T_{CMB}, a noise pattern, n, and a set of foreground components X_i:

$$T_{BEAST} = T_{CMB} + n + \sum_i \alpha_i X_i, \tag{1}$$

where α_i are the coupling constants which transform the foreground template intensities into antenna temperature at the BEAST frequencies. These constants correspond to the correlation coefficients that minimize a χ^2 expression of the type

$$\chi^2 = \sum_{jk} \Big[T_{BEAST} - \sum_i (\alpha_i X_i) \Big]_j C^{-1}_{jk} \Big[T_{BEAST} - \sum_i (\alpha_i X_i) \Big]_k, \tag{2}$$

where C_{jk} is the covariance matrix of the BEAST data. Since the noise pattern and the CMB anisotropy maps are uncorrelated Gaussian variables with zero mean, uncorrelated with the foreground templates, and also considering n and T_{CMB} as noise, the T_{BEAST} temperature fluctuations correspond to a mapping of the fluctuations in the distribution

of the Galactic emission. C_{jk} also accounts for any chance alignment between CMB and the Galactic templates which dominate the uncertainty in the coupling constants. Similar analysis has been applied to data sets from different experiments that characterize CMB fluctuations (Bennett et al. 1993; Kogut et al. 1996a, b; de Oliveira-Costa et al. 1997, 1999; Hamilton & Ganga 2001 and Mukherjee et al. 2002, 2003).

Considering the X_i vectors as constants, the C_{jk} matrix is given by

$$C = \langle T_{BEAST} T_{BEAST}^T \rangle - \langle T_{BEAST} \rangle \langle T_{BEAST}^T \rangle = \langle T_{CMB} T_{CMB}^T \rangle + \langle n n^T \rangle = C_{CMB} + C_n, \quad (3)$$

the sum of the covariance matrix modeling the CMB signal and the noise covariance matrix. Minimizing the χ^2, the best estimates of α_i are obtained as the solutions to the system of equations

$$(X) C^{-1} (X)^T \tilde{\alpha} = (X) C^{-1} (T_{BEAST})^T \quad (4)$$

with a variance given by

$$\sigma_{\tilde{\alpha}}^2 = [(X) C^{-1} (X)^T]^{-1}. \quad (5)$$

In Equations (4) and (5), the X terms correspond to $(M \times N)$ arrays, where M is the number of foreground templates simultaneously analyzed and N is the number of pixels in the maps, and the $\tilde{\alpha}$ term corresponds to a $(M \times 1)$ vector representing the unknown α_i parameters to be evaluated.

Finally, we estimated the level of Galactic contribution to the BEAST maps by comparing the rms of the fluctuations in the Galactic templates, scaled by their coupling constants ($\Delta T \equiv \tilde{\alpha} \cdot \sigma_{Gal}$), to the rms of the BEAST temperature fluctuations in the corresponding Ka- and Q-band maps. The rms values follow directly from the estimates of the individual map variances

$$\sigma_{Gal,i}^2 = \frac{(X_i)^T (X_i)}{N}, \quad (6)$$

for each Galactic contaminant template and

$$\sigma_{BEAST}^2 = \frac{(T_{BEAST})^T (T_{BEAST})}{N}, \quad (7)$$

for the BEAST maps.

5. ANALYSIS AND RESULTS

The two BEAST maps at Ka- and Q-band were divided, along the RA axis, in 24 sections of one-hour (RA), beginning at RA=0 h, each with $\sim$ 7900 pixels, and were independently analyzed. To characterize the correlation with the foreground templates, we calculated the Pearson's linear correlation coefficient for the 24 sub-maps for each of the two BEAST maps. The results are presented in Tables 1 to 6 and Figures 3 to 5. We should point out that the templates we used do not necessarily trace the behavior of the individual Galactic foreground contaminants at BEAST frequencies, even though the generally low values of the correlation coefficients over the 1-hour RA section may suggest this.

For the free-free emission, in at least two regions in both BEAST maps, identified as regions 3 ($3\,\mathrm{h} \leq \mathrm{RA} < 4\,\mathrm{h}$) and 4 ($4\,\mathrm{h} \leq \mathrm{RA} < 5\,\mathrm{h}$) in Tables 1 and 2, the value of the correlation coefficient was above 0.45 for both bands ($\mathrm{p} < 0.0001$), high enough to consider them as highly contaminated by the free-free emission. It is possible to see, in the same tables, that the percentage of temperature contribution of the free-free emission (as traced by the Hα template) to the corresponding BEAST map regions varies between 49.0% and 56.5% (Ka-band) and between 48.1% and 64.4% (Q-band).

In the same tables, we present the values of the α parameter as obtained from Equation 4. For the regions mentioned above, the α parameter varies from (6.4 ± 0.4) μK/R to (8.3 ± 0.4) μK/R for the Ka-band, and from (3.3 ± 0.2) μK/R to (4.1 ± 0.2) μK/R for the Q-band. These values agree with the theoretical results presented by Dickinson et al. (2003), for an electronic temperature $\mathrm{T}_e \sim 10^4$ K.

For synchrotron emission, the correlation coefficient was always below 0.15, except for region 16 ($16\,\mathrm{h} \leq \mathrm{RA} < 17\,\mathrm{h}$) in the Ka-band and regions 16 ($16\,\mathrm{h} \leq \mathrm{RA} < 17\,\mathrm{h}$) and 23 ($23\,\mathrm{h} \leq \mathrm{RA} < 24\,\mathrm{h}$) in Q-band, in Tables 3 and 4. For these regions the constribution in temperature corresponds to 16.8 % in the Ka-band, and varies between 16.7% and 23.0% in the Q-band.

For thermal dust emission, the same two regions as in the free-free emission case in both BEAST maps, identified as regions 3 and 4 in Tables 5 and 6, present values of the correlation coefficient above 0.42 for both bands ($\mathrm{p} < 0.0001$), high enough to consider them as highly contaminated by the thermal dust emission. The percentage of temperature contribution of the thermal dust emission to the corresponding BEAST map regions varies between 42.1% and 67.4% (Ka-band), and between 47.0% and 67.5% (Q-band).

The α parameter values obtained for the regions mentioned above vary from (30.1 ± 2.1) μK/(MJy/sr) to $(45.0.0 \pm 2.0)$ μK/(MJy/sr) for the Ka-band and from (14.6 ± 1.2) μK/(MJy/sr) to (24.0 ± 1.1) μK/(MJy/sr) for the Q-band.

Due to the large number of pixels in the BEAST maps, we are able to determine the α values corresponding to different regions of the Galaxy, which allow us to take into account spatial variations in the Galaxy foreground emission. For instance, we focused on one interesting feature found in BEAST maps, which we called "the bar" (Meinhold et al. 2003), centered around RA = 4.04 h (60.6°) and $\delta = 36.2°$, shown in Figure 6, and performed the same calculation for the region located between $58.3° < \mathrm{RA} < 62.7°$ and $34.7° < \delta < 38.0°$ obtaining as results (7.51 ± 0.31) μK/R at 30 GHz and (3.76 ± 0.17) μK/R at 41.5 GHz. The corresponding Pearson's correlation coefficients were 0.648 (Ka-band) and 0.623 (Q-band) (875 pixels; $p < 0.0001$).

In order to determine regions of the sky to be avoided for BEAST CMB analysis due to Galactic foreground contamination, we applied the method outlined in the previous section to evaluate the Galactic foreground contribution in our data set. BEAST beams crossed twice the Galactic Plane in the observational campaign at WMRS. This allows us to examine in detail the extent of the Galactic contamination in our data. We began with a 2.5° cut above and below the Galactic Plane and estimated the individual contribution of each foreground component in the remaining part of the BEAST maps. We set a $|b| = 5°$ step for further cuts. Tables 7 and 8 show the results of this procedure. The number of pixels left in the BEAST maps is presented in the second column of Tables 7 and 8. Columns 4, 6, and 8, in both tables, present the percentual temperature contribution of each foreground component, estimated from the templates, while columns 3, 5, and 7 show the corresponding α parameters for the three foregrounds after each sucessive Galactic Plane remotion. It is clear from these tables that the Galactic foreground contamination is negligible after a $|b| = 17.5°$ Galactic cut. This cut was then applied to our data set in order to generate BEAST CMB maps (Meinhold et al. 2003) and estimate CMB power spectrum (O'Dwyer et al. 2004).

We want to thank the White Mountain Research Station staff for the very important support during BEAST operation. This work was funded by NASA grants NAG5-4078, NAG5-9073, and NAG5-4185, and by NSF grants 9813920 and 0118297. In addition we were supported by the White Mountain Research Station, the California Space Institute (CalSpace) and the UCSB Office of Research. The development and operations of BEAST were supported by NASA Office of Space Sciences, the National Science Foundation, University of California White Mountain Research Station, and the California Space Institute (CalSpace). J.M. was supported by FAPESP grants 01/13235-9 and 02/04871-1. T.V. was partially supported by FAPESP grant 00/06770-2 and by CNPq grants 466184/00-0

and 302266/88-7-FA. C.A.W. was partially supported by CNPq grant 300409/97-4-FA and FAPESP grants 00/06770-2 and 96/06501-4. N.F. and A.P. were partially supported by CNPq grant 470531/2001-0. Some of the results in this paper have been derived using the HEALPix (Górski et al. 1999) package.

REFERENCES

Banday, A.J. et al., 2003, MNRAS, 345, 897.

Bennett, C.L. et al., 1993, ApJ, 414, L77.

Bennett, C.L. et al., 2003, ApJS, 148, 97.

Childers, J. et al., 2004, to be submitted to ApJ.

Dennison, B., Simonetti, J.H. & Topasna, G., 1998, PASA, 15, 147.

de Oliveira-Costa, A. et al., 1997, ApJ, 482, L17.

de Oliveira-Costa, A. et al., 1999, ApJ, 527, L9.

Dickinson, C., Davies, R.D. & Davis, R.J., 2003, MNRAS, 341, 369.

Draine, B.T. & Lazarian, A., 1998, ApJ, 494, L19.

Figueiredo, N. et al., 2004, submitted to ApJ.

Finkbeiner, D.P., 2003, astro-ph/0301558, ApJS, in press.

Finkbeiner, D.P., Davis, M. & Schlegel, D.J., 1999, ApJ, 524, 867.

Górski, K.M., Hivon, E. & Wandelt, B.D., 1999, in Proceedings of the MPA/ESO Cosmology Conference on Evolution of Large Scale Structure. Eds. A.J. Banday, R.S. Sheth & L. da Costa.

Gaustad, J.E., McCullough, P.R., Rosing, W. & Van Buren, D.,2001, PASP, 113, 1326.

Hamilton, J.Ch. & Ganga, K.M., 2001, A&A, 368, 760.

Haslam, C.G.T., Salter, C.J., Stoffel, H. & Wilson, W., 1982, A&AS, 47, 1.

Kogut, A. et al., 1996, ApJ, 460, 1.

Kogut, A. et al., 1996, ApJ Letters, 464, L5.

Meinhold, P. et al., 2003, astro-ph/0302034, submitted to ApJ.

Mukherjee, P. et al., 2002, ApJ, 579, 83.

Mukherjee, P. et al., 2003, ApJ, 592, 692.

O'Dwyer, I. et al., 2004, astro-ph/0312610, submitted to ApJ.

Platania, P. et al., 2003, A&A, 410, 847.

Reynolds, R.J., Haffner, L.M. & Madsen, G.J., 2002, in "Galaxies: the third dimension", ASP Conf. Series, vol. 282. Eds. M. Rosado, L. Binette & L. Arias, in press.

Schlegel, D.J., Finkbeiner, D.P. & Davis, M., 1998, ApJ, 500, 525.

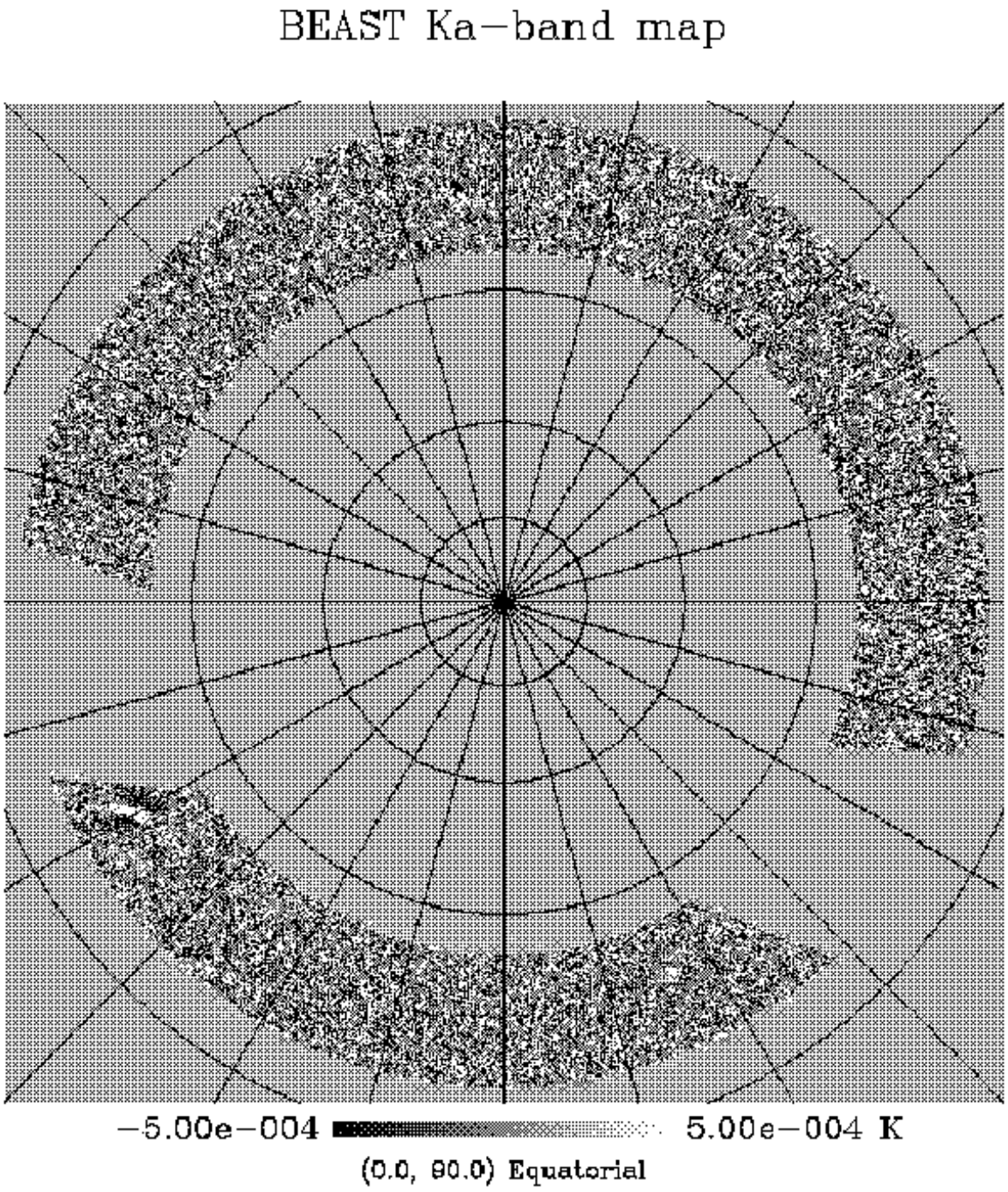

Fig. 1.— BEAST Ka-band map in gnomonic projection. RA = 0 h is at the bottom, increasing clockwise, and the North Celestial Pole is at the center. Each graticule division corresponds to 15° x 15° (RA, δ).

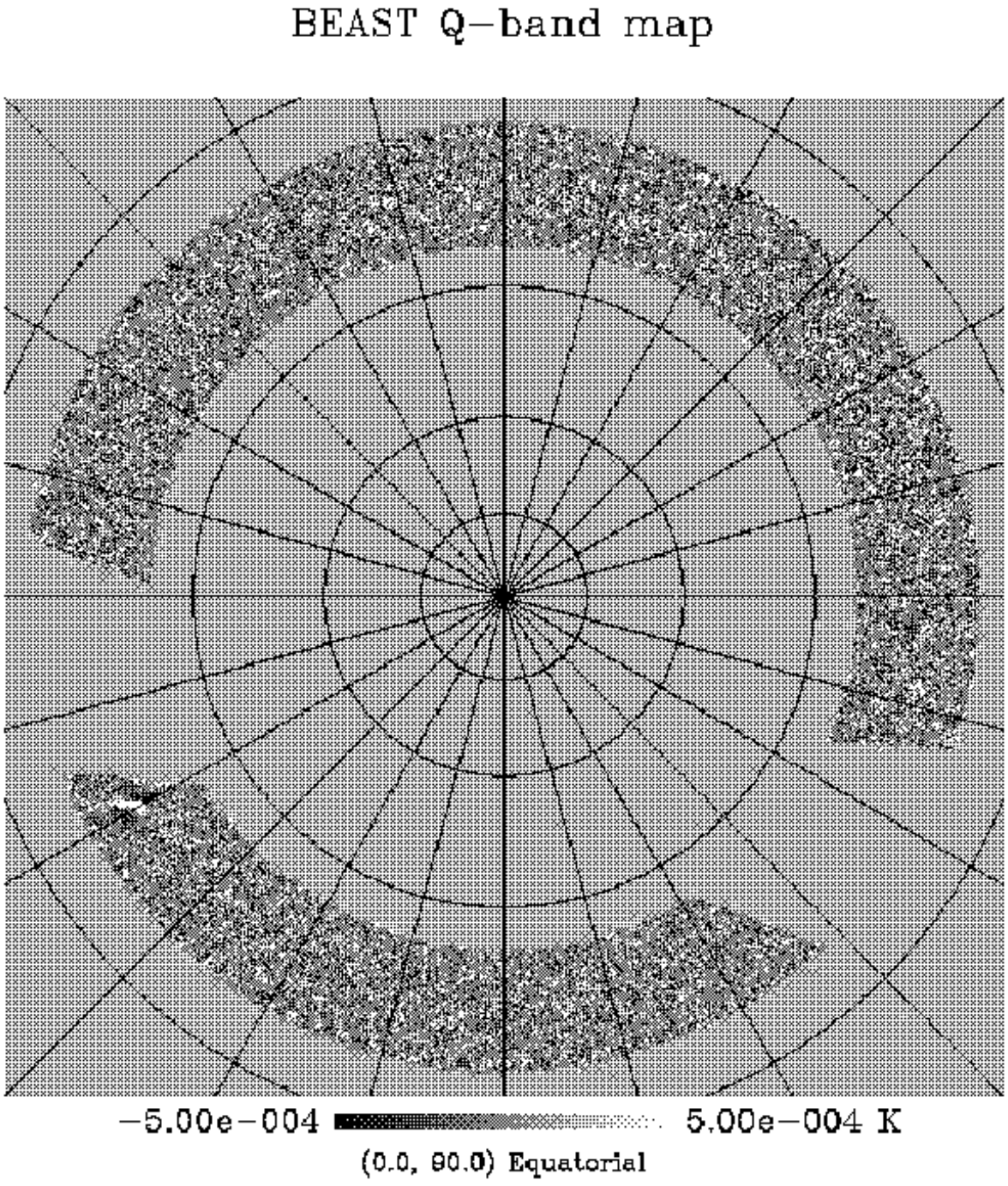

Fig. 2.— BEAST Q-band map in gnomonic projection. RA = 0 h is at the bottom, increasing clockwise, and the North Celestial Pole is at the center. Each graticule division corresponds to 15° x 15° (RA, δ).

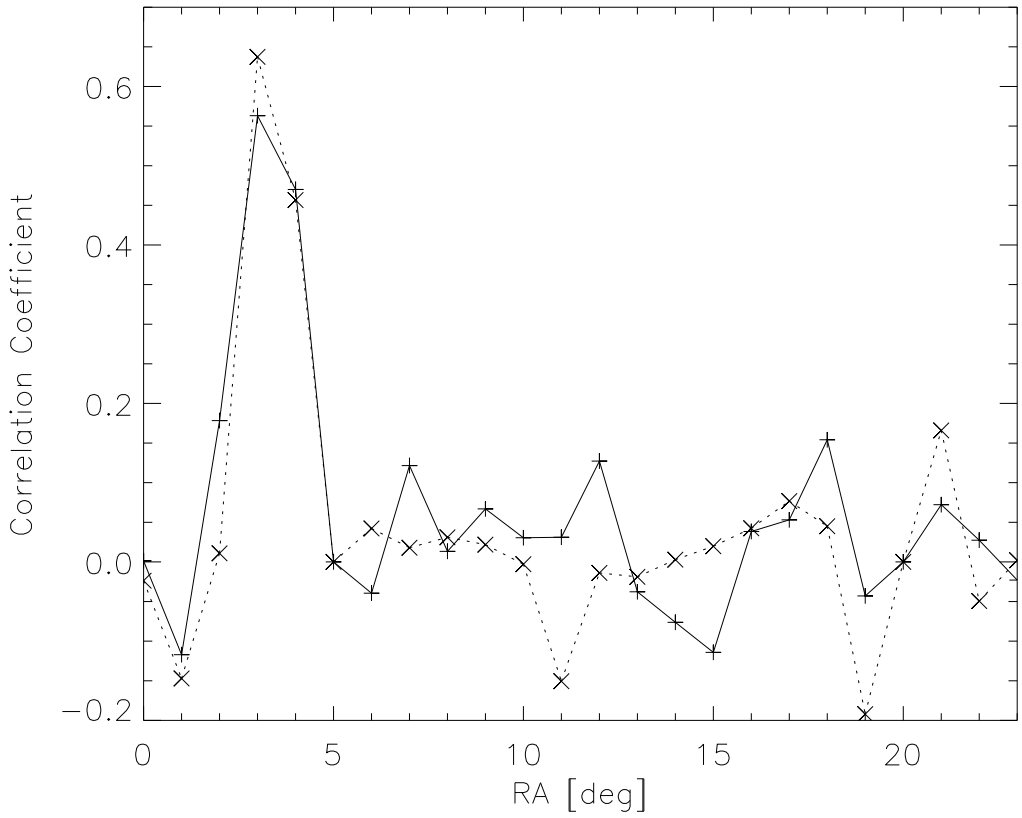

Fig. 3.— Pearson's coefficients for the linear correlation between BEAST Ka-band map and Hα template (dotted line), and BEAST Q-band map and Hα template (solid line).

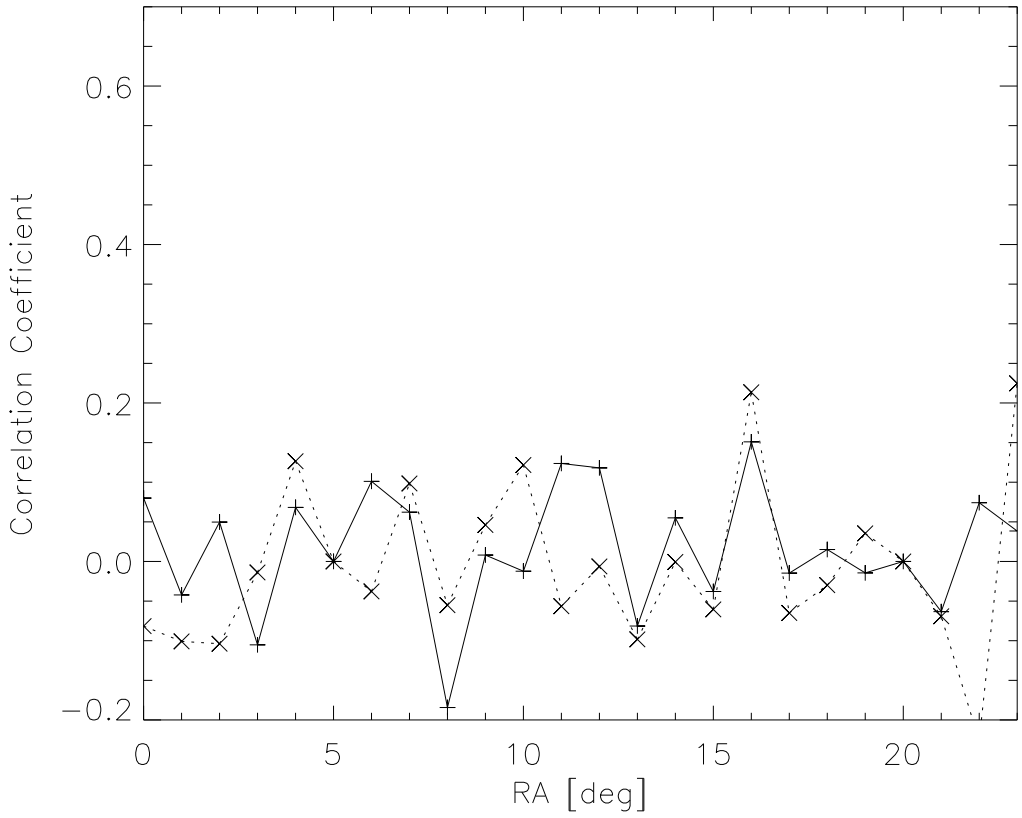

Fig. 4.— Pearson's coefficients for the linear correlation between BEAST Ka-band map and synchrotron 408 MHz template (dotted line), and BEAST Q-band map and synchrotron 408 MHz template (solid line).

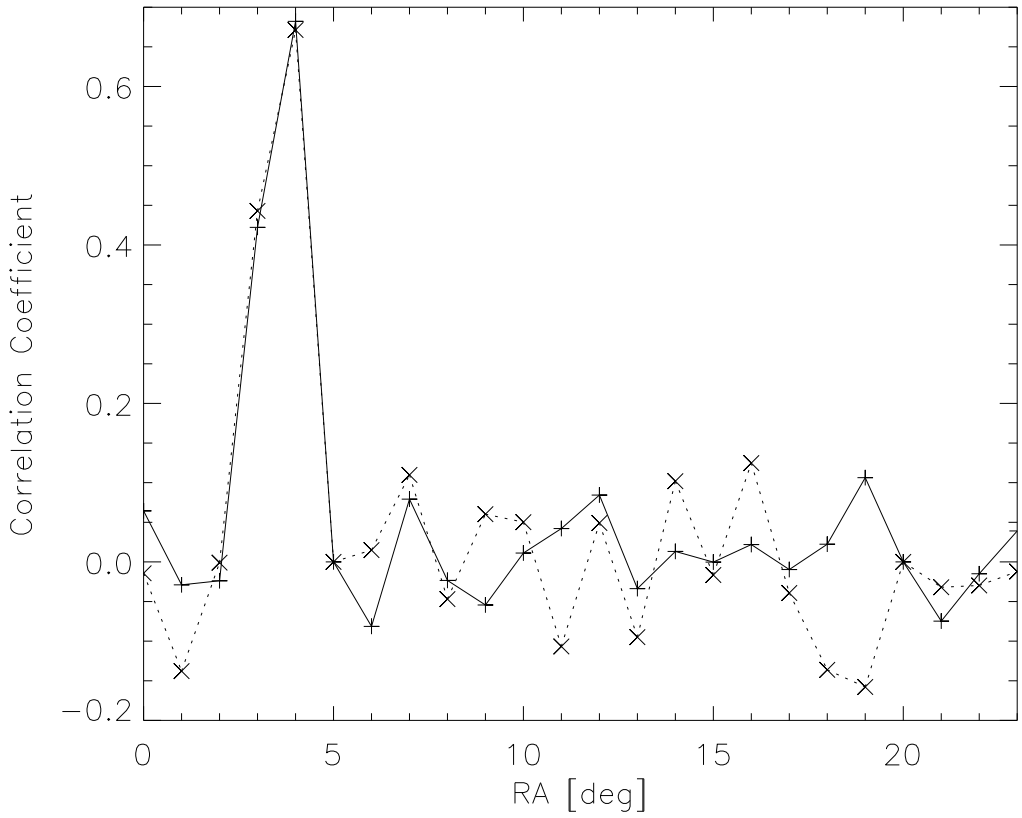

Fig. 5.— Pearson's coefficients for the linear correlation between BEAST Ka-band map and dust template (dotted line), and BEAST Q-band map and dust template (solid line).

(a) "The Bar" (BEAST Ka−band map)

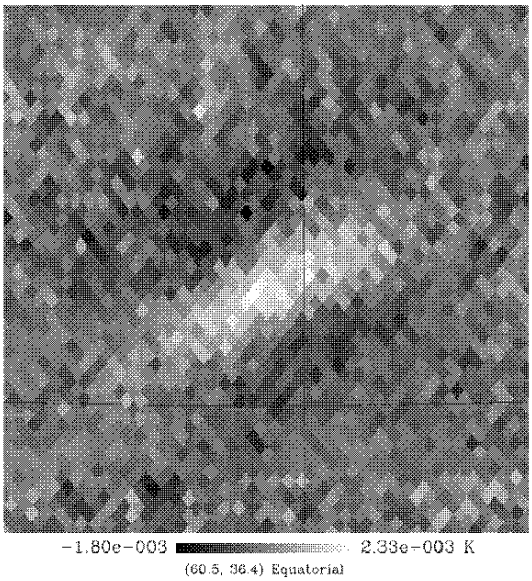

(b) "The Bar" (BEAST Q−band map)

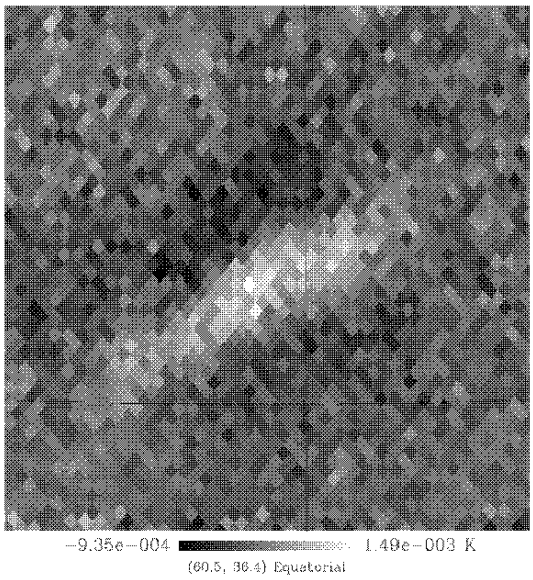

(c) "The Bar" (beasted H−alpha Q−band map)

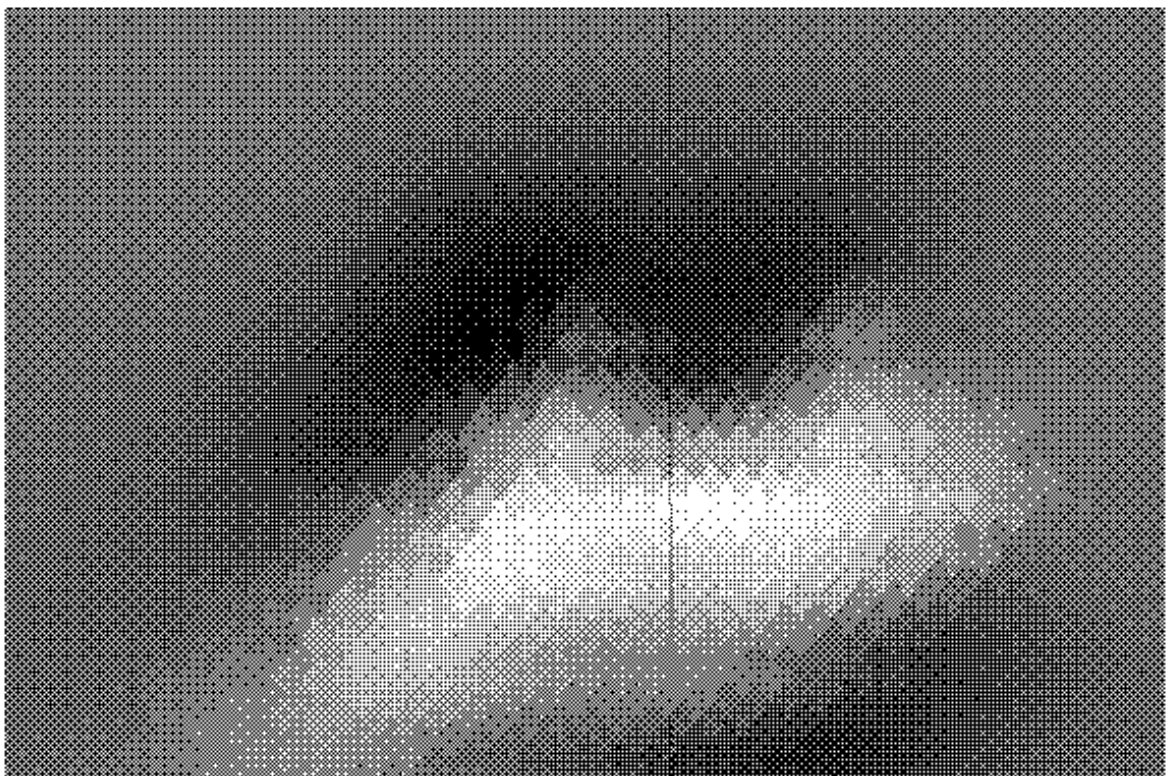

Table 1. Correlation results between BEAST Ka-band map and Hα template

Section	Number of pixels	Correlation Coeff.	Probability [%]	$\tilde{\alpha}$ [μK/R]	$\sigma_{\tilde{\alpha}}$ [μK/R]	σ_{Gal} [R]	$\Delta T \equiv \tilde{\alpha} \cdot \sigma_{Gal}$ [μK]	$\Delta T/\sigma_B$ [%]
0	7951	0.0013	45.41	-0.334	9.848	0.343	-0.11	-0.14
1	7952	-0.1171	< 0.01	-50.643	18.460	0.214	-10.84	-12.00
2	7951	0.1784	< 0.01	50.981	12.498	0.310	15.78	17.08
3	7780	0.5631	< 0.01	8.318	0.440	9.241	76.87	56.48
4	2009	0.4701	< 0.01	6.393	0.391	20.624	131.84	49.00
6	5467	-0.0395	0.17	-25.822	28.888	0.181	-4.68	-4.95
7	7952	0.1215	< 0.01	101.153	41.827	0.102	10.34	12.00
8	7951	0.0133	11.80	19.786	71.587	0.058	1.14	1.18
9	7905	0.0669	< 0.01	302.061	127.176	0.032	9.55	9.57
10	7952	0.0305	0.33	112.272	106.123	0.038	4.32	4.34
11	7951	0.0311	0.28	122.695	133.724	0.031	3.83	3.68
12	7905	0.1272	< 0.01	529.030	159.984	0.025	13.13	13.00
13	7951	-0.0377	0.04	-110.799	101.603	0.040	-4.46	-3.53
14	7949	-0.0763	< 0.01	-195.850	112.354	0.038	-7.43	-6.58
15	7899	-0.1142	< 0.01	-303.971	112.344	0.038	-11.46	-11.16
16	7947	0.0383	0.03	113.628	80.361	0.056	6.36	5.34
17	7944	0.0531	< 0.01	46.845	44.450	0.098	4.60	4.43
18	7821	0.1542	< 0.01	54.151	13.304	0.316	17.09	14.58
19	3211	-0.0430	0.75	-4.796	13.634	0.493	-2.36	-2.09
21	4134	0.0722	< 0.01	5.826	3.541	1.449	8.44	8.74
22	7952	0.0274	0.73	1.547	1.219	2.883	4.46	4.98
23	7905	-0.0229	2.08	-17.183	16.594	0.219	-3.76	-4.41

Table 2. Correlation results between BEAST Q-band map and Hα template

Section	Number of pixels	Correlation Coeff.	Probability [%]	$\tilde{\alpha}$ [μK/R]	$\sigma_{\tilde{\alpha}}$ [μK/R]	σ_{Gal} [R]	$\Delta T \equiv \tilde{\alpha} \cdot \sigma_{Gal}$ [μK]	$\Delta T/\sigma_B$ [%]
0	7866	-0.0237	1.77	-3.628	7.307	0.231	-0.84	-1.84
1	7866	-0.1471	< 0.01	-29.253	10.543	0.223	-6.53	-13.56
2	7866	0.0108	16.87	-0.512	6.510	0.314	-0.16	-0.34
3	7723	0.6373	< 0.01	4.093	0.239	9.907	40.54	64.39
4	2059	0.4567	< 0.01	3.284	0.211	21.961	72.13	48.08
6	5361	0.0422	0.10	13.347	14.109	0.193	2.58	5.52
7	7866	0.0179	5.65	31.502	21.608	0.108	3.40	6.97
8	7866	0.0311	0.29	50.767	41.305	0.061	3.07	6.55
9	7820	0.0219	2.67	122.951	72.972	0.033	4.07	7.90
10	7866	-0.0029	39.81	21.357	57.900	0.040	0.86	1.49
11	7866	-0.1505	< 0.01	-215.064	68.664	0.032	-6.92	-15.75
12	7820	-0.0139	11.02	-92.942	92.754	0.025	-2.34	-3.74
13	7866	-0.0189	4.72	-56.237	59.903	0.042	-2.35	-4.09
14	7866	0.0028	40.15	-48.228	64.271	0.039	-1.89	-2.90
15	7820	0.0198	3.99	-26.230	63.992	0.039	-1.03	-1.65
16	7866	0.0424	0.01	11.437	42.818	0.060	0.69	0.89
17	7866	0.0767	< 0.01	52.133	24.553	0.103	5.36	7.74
18	7820	0.0450	< 0.01	1.002	7.716	0.332	0.33	0.64
19	3135	-0.1921	< 0.01	-26.138	7.276	0.518	-13.55	-24.03
21	4187	0.1659	< 0.01	5.066	1.926	1.510	7.65	17.38
22	7866	-0.0494	< 0.01	-0.202	0.727	2.953	-0.60	-1.26
23	7820	0.0020	42.92	5.084	9.601	0.225	1.15	2.38

Table 3. Correlation results between BEAST Ka-band map and synchrotron template

Section	Number of pixels	Correlation Coeff.	Probability [%]	$\tilde{\alpha}$ [μK/K]	$\sigma_{\tilde{\alpha}}$ [μK/K]	σ_{Gal} [K]	$\Delta T \equiv \tilde{\alpha} \cdot \sigma_{Gal}$ [μK]	$\Delta T/\sigma_B$ [%]
0	7951	0.0800	< 0.01	34.971	19.561	0.190	6.64	8.25
1	7952	-0.0422	0.01	-21.833	27.558	0.133	-2.91	-3.23
2	7951	0.0497	< 0.01	26.748	22.201	0.172	4.60	4.98
3	7780	-0.1052	< 0.01	-88.337	23.274	0.166	-14.65	-10.76
4	2009	0.0683	0.11	124.116	36.736	0.204	25.35	9.42
6	5467	0.1011	< 0.01	56.083	28.984	0.175	9.83	10.40
7	7952	0.0622	< 0.01	27.298	27.256	0.154	4.21	4.88
8	7951	-0.1843	< 0.01	-101.841	25.641	0.161	-16.39	-16.87
9	7905	0.0081	23.59	0.660	23.600	0.169	0.11	0.11
10	7952	-0.0123	13.66	-5.424	28.091	0.149	-0.81	-0.81
11	7951	0.1237	< 0.01	65.980	28.340	0.148	9.73	9.35
12	7905	0.1181	< 0.01	88.272	27.529	0.144	12.71	12.57
13	7951	-0.0814	< 0.01	-52.196	25.107	0.162	-8.46	-6.69
14	7949	0.0550	< 0.01	31.858	26.020	0.163	5.20	4.60
15	7899	-0.0379	0.04	-25.449	25.558	0.159	-4.06	-3.95
16	7947	0.1510	< 0.01	126.873	27.972	0.157	19.98	16.78
17	7944	-0.0147	9.50	3.388	23.043	0.189	0.64	0.62
18	7821	0.0151	9.07	4.883	15.154	0.280	1.37	1.17
19	3211	-0.0144	20.66	1.086	4.729	1.382	1.50	1.33
21	4134	-0.0633	< 0.01	-26.173	18.433	0.284	-7.44	-7.70
22	7952	0.0742	< 0.01	22.775	15.579	0.227	5.17	5.77
23	7905	0.0385	0.03	12.597	20.843	0.183	2.30	2.70

Table 4. Correlation results between BEAST Q-band map and synchrotron template

Section	Number of pixels	Correlation Coeff.	Probability [%]	$\tilde{\alpha}$ [μK/K]	$\sigma_{\tilde{\alpha}}$ [μK/K]	σ_{Gal} [K]	$\Delta T \equiv \tilde{\alpha} \cdot \sigma_{Gal}$ [μK]	$\Delta T/\sigma_B$ [%]
0	7866	-0.0816	< 0.01	-22.379	11.054	0.199	-4.45	-9.79
1	7866	-0.1009	< 0.01	-39.178	15.506	0.135	-5.30	-11.00
2	7866	-0.1038	< 0.01	-28.106	12.827	0.177	-4.98	-10.40
3	7723	-0.0139	11.12	2.197	11.932	0.171	0.37	0.60
4	2059	0.1265	< 0.01	117.535	19.753	0.219	25.79	17.20
6	5361	-0.0378	0.28	-9.900	16.454	0.180	-1.78	-3.82
7	7866	0.0985	< 0.01	43.436	14.335	0.160	6.97	14.29
8	7866	-0.0551	< 0.01	-13.540	14.155	0.164	-2.23	-4.74
9	7820	0.0461	< 0.01	19.541	12.704	0.174	3.40	6.61
10	7866	0.1218	< 0.01	47.519	15.324	0.156	7.44	12.91
11	7866	-0.0565	< 0.01	-26.170	14.895	0.156	-4.08	-9.29
12	7820	-0.0063	28.90	1.703	16.089	0.143	0.24	0.39
13	7866	-0.0983	< 0.01	-38.581	14.201	0.166	-6.39	-11.13
14	7866	-0.0006	47.78	9.103	14.197	0.170	1.55	2.38
15	7820	-0.0605	< 0.01	-24.101	14.103	0.167	-4.02	-6.41
16	7866	0.2135	< 0.01	79.253	16.046	0.163	12.89	16.70
17	7866	-0.0650	< 0.01	-5.030	12.205	0.200	-1.00	-1.45
18	7820	-0.0299	0.41	-8.900	8.736	0.297	-2.64	-5.09
19	3135	0.0355	2.35	0.257	3.491	1.069	0.27	0.49
21	4187	-0.0692	< 0.01	-13.168	10.879	0.296	-3.90	-8.86
22	7866	-0.2265	< 0.01	-49.490	9.234	0.228	-11.26	-23.78
23	7820	0.2248	< 0.01	58.077	11.559	0.191	11.08	23.05

Table 5. Correlation results between BEAST Ka-band map and dust template

Section	Number of pixels	Correlation Coeff.	Probability [%]	$\tilde{\alpha}$ [μK/(MJy/sr)]	$\sigma_{\tilde{\alpha}}$ [μK/(MJy/sr)]	σ_{Gal} [MJy/sr]	$\Delta T \equiv \tilde{\alpha} \cdot \sigma_{Gal}$ [μK]	$\Delta T/\sigma_B$ [%]
0	7951	0.0644	< 0.01	14.201	10.097	0.351	4.98	6.19
1	7952	-0.0289	0.50	-10.193	23.609	0.164	-1.67	-1.85
2	7951	-0.0238	1.69	-6.329	18.616	0.211	-1.33	-1.44
3	7780	0.4222	< 0.01	30.055	2.126	1.905	57.26	42.07
4	2009	0.6822	< 0.01	45.005	1.952	4.029	181.31	67.38
6	5467	-0.0814	< 0.01	-17.635	15.580	0.325	-5.74	-6.07
7	7952	0.0792	< 0.01	59.063	30.928	0.139	8.23	9.55
8	7951	-0.0234	1.85	1.813	39.772	0.104	0.19	0.19
9	7905	-0.0544	< 0.01	-135.524	98.548	0.040	-5.43	-5.44
10	7952	0.0112	15.98	41.186	81.962	0.051	2.09	2.10
11	7951	0.0421	0.01	77.948	58.581	0.070	5.43	5.21
12	7905	0.0843	< 0.01	125.368	59.849	0.065	8.17	8.09
13	7951	-0.0337	0.13	-103.639	89.066	0.048	-4.94	-3.91
14	7949	0.0132	11.94	16.996	74.317	0.058	0.99	0.87
15	7899	-0.0003	49.10	16.916	70.642	0.059	1.00	0.98
16	7947	0.0219	2.55	9.961	70.057	0.065	0.65	0.55
17	7944	-0.0096	19.57	-8.173	34.141	0.129	-1.06	-1.02
18	7821	0.0223	2.42	3.532	14.848	0.289	1.02	0.87
19	3211	0.1063	< 0.01	23.486	12.282	0.498	11.70	10.38
21	4134	-0.0747	< 0.01	-7.967	7.640	0.701	-5.59	-5.78
22	7952	-0.0149	9.17	-0.977	8.226	0.450	-0.44	-0.49
23	7905	0.0390	0.03	7.824	11.336	0.340	2.66	3.12

Table 6. Correlation results between BEAST Q-band map and dust template

Section	Number of pixels	Correlation Coeff.	Probability [%]	$\tilde{\alpha}$ [μK/(MJy/sr)]	$\sigma_{\tilde{\alpha}}$ [μK/(MJy/sr)]	σ_{Gal} [MJy/sr]	$\Delta T \equiv \tilde{\alpha} \cdot \sigma_{Gal}$ [μK]	$\Delta T/\sigma_B$ [%]
0	7866	-0.0143	10.21	-1.108	5.800	0.308	-0.34	-0.75
1	7866	-0.1378	< 0.01	-33.899	12.862	0.174	-5.90	-12.25
2	7866	-0.0010	46.51	-2.607	11.030	0.222	-0.58	-1.21
3	7723	0.4429	< 0.01	14.550	1.183	2.034	29.60	47.02
4	2059	0.6713	< 0.01	23.965	1.074	4.224	101.22	67.48
6	5361	0.0149	13.72	3.324	8.136	0.348	1.16	2.48
7	7866	0.1098	< 0.01	39.823	17.641	0.144	5.73	11.75
8	7866	-0.0469	< 0.01	-9.518	22.134	0.108	-1.03	-2.20
9	7820	0.0602	< 0.01	60.040	54.567	0.041	2.46	4.78
10	7866	0.0502	< 0.01	79.322	46.521	0.054	4.27	7.42
11	7866	-0.1068	< 0.01	-91.406	33.964	0.069	-6.30	-14.33
12	7820	0.0491	< 0.01	27.629	35.994	0.065	1.80	2.88
13	7866	-0.0949	< 0.01	-139.652	49.966	0.049	-6.88	-12.00
14	7866	0.1019	< 0.01	14.798	39.502	0.062	0.92	1.41
15	7820	-0.0165	7.19	-23.783	40.560	0.061	-1.45	-2.32
16	7866	0.1248	< 0.01	121.100	41.298	0.068	8.21	10.63
17	7866	-0.0393	0.02	-37.852	19.775	0.134	-5.07	-7.33
18	7820	-0.1362	< 0.01	-19.961	7.869	0.293	-5.86	-11.28
19	3135	-0.1578	< 0.01	-19.227	7.309	0.497	-9.55	-16.93
21	4187	-0.0319	1.94	0.070	4.039	0.731	0.05	0.12
22	7866	-0.0297	0.42	2.066	4.462	0.458	0.95	2.00
23	7820	-0.0121	14.17	1.747	6.321	0.371	0.65	1.35

Table 7. Correlation results between BEAST Ka-band map and foreground templates after different cuts in galactic latitude

Galactic cut |b| [°]	Number of pixels	$\tilde{\alpha}_{H\alpha}$ [μK/R]	$\Delta T_{H\alpha}/\sigma_B$ [%]	$\tilde{\alpha}_{sync}$ [μK/K]	$\Delta T_{sync}/\sigma_B$ [%]	$\tilde{\alpha}_{dust}$ [μK/(MJy/sr)]	$\Delta T_{dust}/\sigma_B$ [%]
2.50	182349	5.5 ± 0.2	14.11	4.2 ± 0.1	34.61	11.9 ± 0.3	25.53
7.50	165947	6.9 ± 0.3	19.99	1.9 ± 0.7	2.16	10.9 ± 0.6	13.46
12.50	148942	8.3 ± 0.4	15.89	14.0 ± 5.1	2.44	35.0 ± 2.2	13.86
17.50	130519	-4.3 ± 2.6	-1.57	8.2 ± 5.8	1.37	4.4 ± 4.7	0.88
22.50	106959	-5.0 ± 12.0	-0.45	10.0 ± 6.7	1.63	9.5 ± 8.7	1.2

Table 8. Correlation results between BEAST Q-band map and foreground templates after different cuts in galactic latitude

Galactic cut |b| [°]	Number of pixels	$\tilde{\alpha}_{H\alpha}$ [μK/R]	$\Delta T_{H\alpha}/\sigma_B$ [%]	$\tilde{\alpha}_{sync}$ [μK/K]	$\Delta T_{sync}/\sigma_B$ [%]	$\tilde{\alpha}_{dust}$ [μK/(MJy/sr)]	$\Delta T_{dust}/\sigma_B$ [%]
2.50	180412	2.4 ± 0.1	12.47	1.73 ± 0.04	27.42	7.0 ± 0.2	29.45
7.50	164235	3.4 ± 0.2	20.02	1.55 ± 0.32	3.42	5.1 ± 0.4	11.99
12.50	147474	4.2 ± 0.2	16.14	-3.7 ± 2.9	-1.24	16.2 ± 1.2	12.65
17.50	129353	-3.3 ± 1.5	-2.35	-3.0 ± 3.2	-0.95	-3.7 ± 2.6	-1.46
22.50	106350	-15.0 ± 6.9	-2.47	1.6 ± 3.8	0.46	-3.9 ± 4.9	-0.90